ADVANCED MATERIALS TECHNOLOGIES
www.advmattechnol.de

Streamlined Inkjet-Printing of Stretchable Organic Photodetectors

*Mervin Seiberlich, Christian Rainer, Leon Skarjan, Luis Arturo Ruiz-Preciado, Aleksandr Perevedentsev, Kai Xia, Peter Krebsbach, Stefan Schlisske, Uli Lemmer, and Gerardo Hernandez-Sosa**

The rapid development of the Internet of Things (IoT), artificial intelligence, robotics, and wearable electronics has created new challenges and increased the demand for advanced sensing technologies. These sensors must not only exhibit tailored performance but also offer new properties like stretchability and flexibility while being compatible with industrial manufacturing. In this work, a streamlined and simplified method is introduced for fabricating stretchable Organic Photodiodes (OPDs) relying solely on industry-grade inkjet-printing. It is demonstrated that printed stiff islands effectively decouple strain from the stretched substrate and serve as a chemically resistant and mechanically rigid platform for printed OPDs. Printing difficulties that arose while processing the Ag electrodes on the curved island surfaces are overcome by a two-step printing process. Finally, the study reports fully printed OPDs exhibiting peak responsivities ($\lambda = 730$ nm) of 340 mA W^{-1} and specific detectivities (D*) of $2.8 \cdot 10^{11}$ Jones at 100 Hz, both measured at −2 V. The light sensors remained functional for over 600 mechanical stretching cycles at strains up to 7%.

1. Introduction

Light detection is essential in many established applications and plays a significant role in fields such as environmental monitoring, medical diagnostics, and signal or imaging systems.[1–3] Furthermore, the rapid development of IoT, artificial intelligence, robotics, and wearable electronics has created a demand for new types of optical sensors that can be seamlessly integrated with these emerging technologies. A promising approach to address this is via the use of industrially-relevant printing technologies such as inkjet-printing or transfer-printing.[4–6] The utilization of printed electronics technology allows for various benefits, such as the freedom of design through precise ink deposition, ultra-thin form factors, the use of flexible substrates, and the versatility of carbon-based semiconductors with a wide range of optoelectronic properties.[4] Printed organic photodiodes (OPDs) recently showcased emerging application examples such as flexible pulse oximeters,[7,8] filterless multichannel optical data transmission,[9] flexible photosensor active matrices,[10,11] or an ultra-flat and completely polymer-based twilight switch.[12] Thus, demonstrating the potential of printed OPDs is key for future technologies that prioritize integrated, customizable, and on-demand fabrication.

Thinking further, a crucial requirement for the integration of optical detection systems into these new technologies is not only their thin form factors and bendability but also their mechanical stretchability.[13–17] This poses particular challenges since mechanical stress can destroy the functionality of thin-film electronic components such as OPDs and their electrical contacts. To address this challenge and render electronic devices strain-resistant, various approaches have been proposed. For instance, stretchable organic photovoltaics and OPDs were achieved by fabricating them as ultra-thin devices on pre-stretched substrates.[8,18–20] Releasing the pre-strain forms microscopic 3D wave structures that enable macroscopic stretching. A second approach is to use intrinsically stretchable materials. For example, intrinsically stretchable polymer diodes,[21]

M. Seiberlich, C. Rainer, L. Skarjan, L. A. Ruiz-Preciado, A. Perevedentsev, K. Xia, P. Krebsbach, S. Schlisske, U. Lemmer, G. Hernandez-Sosa
Light Technology Institute
Karlsruhe Institute of Technology
Engesserstr. 13, 76131 Karlsruhe, Germany
E-mail: gerardo.sosa@kit.edu

M. Seiberlich, C. Rainer, L. Skarjan, L. A. Ruiz-Preciado, A. Perevedentsev, K. Xia, P. Krebsbach, S. Schlisske, U. Lemmer, G. Hernandez-Sosa
InnovationLab
Speyererstr. 4, 69115 Heidelberg, Germany

U. Lemmer, G. Hernandez-Sosa
Institute of Microstructure Technology
Karlsruhe Institute of Technology
Hermann-von-Helmholtz-Platz 1, 76344 Eggenstein-Leopoldshafen, Germany

The ORCID identification number(s) for the author(s) of this article can be found under https://doi.org/10.1002/admt.202401413

DOI: 10.1002/admt.202401413

Organic Light.emitting Diodes (OLEDs),[22,23] phototransistor matrices,[24] nanowire photodetectors,[25] or OPDs[26–29] have recently been presented. However, the selection of materials is limited to those that are intrinsically stretchable, which restricts the transferability of research findings from conventional devices and requires tailored material synthesis. Moreover, the two approaches give rise to difficulties in the interpretation of the photocurrent detection because the effective detector area depends on the strain. Additionally, one of the main manufacturing methods used in these reports besides thermal evaporation was spin-coating, which is not easily scalable for industrial processes. A third approach to fabricate stretchable devices is to combine mechanically rigid islands with elastic substrates.[14,30–35] This approach decouples the strain on the stretchable substrates from the island surface where the device would be fabricated. The islands are interconnected using serpentine structures or stretchable conductors. Examples of this approach include sensors on inflatable catheters,[36] 3D elastic membranes for spatiotemporal cardiac measurements,[37] photo-plethysmography devices integrated in a flexible silicone matrix,[38] stretchable silicon nanoribbon electronics for skin prosthesis,[39] the integration of OPDs and OLEDs for stretchable sensor matrices,[40,41] smart contact lenses,[42] and biodegradable stretchable light-emitting devices.[43] Despite this wide range of applications, the fabrication of island structures has remained relatively complex. This is due to the challenging combination of various manufacturing processes, such as the thermal deposition of electrodes, etching of island structures, and assembly of inorganic or organic electronic devices in the same process.[14,32–35] It is only recently that ink-based coating and printing technologies have been tested in some areas of island production or device integration. For example, rigid islands have been produced by stencil printing[44–47] while laser-cut islands have been combined with inkjet-printed electrodes to form strain-dependent capacitors.[48] In a series of publications, Byun et al. demonstrated the use of inkjet-printed interconnects between islands populated with inorganic devices[49–51] and the embedding of rigid islands in a stretchable substrate using inkjet-printing.[52] However, the full integration of island structures, interconnects, and devices using exclusively printing processes has not yet been achieved. Consequently, from the three discussed approaches, we conclude that there is an opportunity to further refine and optimize the integration of stretchable devices, making them more streamlined and compatible with industrially relevant techniques.[53]

In this work, we demonstrate the fabrication of stretchable inkjet-printed OPDs. This is enabled by the fabrication of stiff islands and interconnects that are inkjet-printed directly onto elastomeric substrates. These structures provide a chemically resistant platform to fabricate the OPDs and, at the same time, a mechanically stable base, shielding the devices from mechanical stress. We investigated and optimized the printing process of these structures, as well as their influence on the mechanical properties of the substrate. Furthermore, we develop and report the printing process and optimal device architecture of the OPDs. Finally, we demonstrate that the electrical conductivity of printed silver (Ag) and the performance of the OPDs are not affected when the substrates are subjected to strains of up to 7%. The presented fully inkjet-printing approach drastically simplifies the fabrication of stretchable OPDs and offers advantageous compatibility with industrial printed and flexible electronics processes. Furthermore, its digital nature provides the potential to be of general use for other types of novel optoelectronic devices in emerging stretchable applications.

2. Results and Discussion

2.1. SU-8 Island Fabrication

Figure 1a,b presents an overview of the fabrication process for the stretchable photodetectors. In the first step, we inkjet-printed the UV-crosslinkable photoresist SU-8 to form rigid islands onto a flexible silicone-based ELASTOSIL elastomer. SU-8 was selected due to its combination of properties, including mechanical and chemical stability, optical transparency, surface tunability by O_2-plasma, biocompatibility, smooth surface, and compatibility with inkjet-printing.[54–56] Following this, the Ag electrical connections and OPDs are successively inkjet-printed on top of the islands. Figure 1c shows the resulting device architecture and materials used. The schematic depicts a rigid island, two connecting serpentines, two contact pads, and the fully printed OPD based on a bulk heterojunction (BHJ) active layer. The chosen BHJ materials are the organic semiconducting polymer P3HT and the non-fullerene acceptor IDTBR (see materials section for full details). Their compatibility with inkjet fabrication of OPDs has been demonstrated in previous works.[10,57] Figure 1d shows the energy alignment of the different materials that facilitate optimized charge extraction and the blocking of injection current to reduce noise.[4,58,59] Figure 1e depicts a photograph of a fully-printed stretchable OPD placed on a curved surface with a radius of 5 mm, showcasing its mechanical flexibility. The upscaling in a small series, as well as the flexibility and stretchability of the devices, is demonstrated in Figure 1f.

The flexible ELASTOSIL substrate proved to be difficult to print on due to its intrinsic low surface energy and a high rms-roughness of 52 nm (see Figure S1, Supporting Information). To illustrate the need for surface treatment, **Figure 2**a shows an example of the contact angle of water on ELASTOSIL with and without O_2 plasma treatment. Sufficient wetting is only achieved with plasma treatment. Figure 2b displays the wetting envelope and its standard deviation, which were calculated by measuring the contact angle of various test fluids. The wetting envelope can serve as a measure of the wettability of different functional inks on the substrate as a function of the polar and dispersive parts of their surface tension.[60–62]

The total surface energy of the substrate was increased from (18 ± 4) mN m^{-1} to (76 ± 2) mN m^{-1} as a result of the plasma treatment. For comparison, we investigated the wetting properties of PDMS and the also commercially available TPU-based substrate Elastollan as alternative substrates (see Figure S2, Supporting Information). We decided to use ELASTOSIL due to its commercial availability as a foil and more homogeneous surface properties.

We printed dual-pass SU-8 structures using a Fujifilm Spectra industrial print head with 128 nozzles (50 pL). In addition,

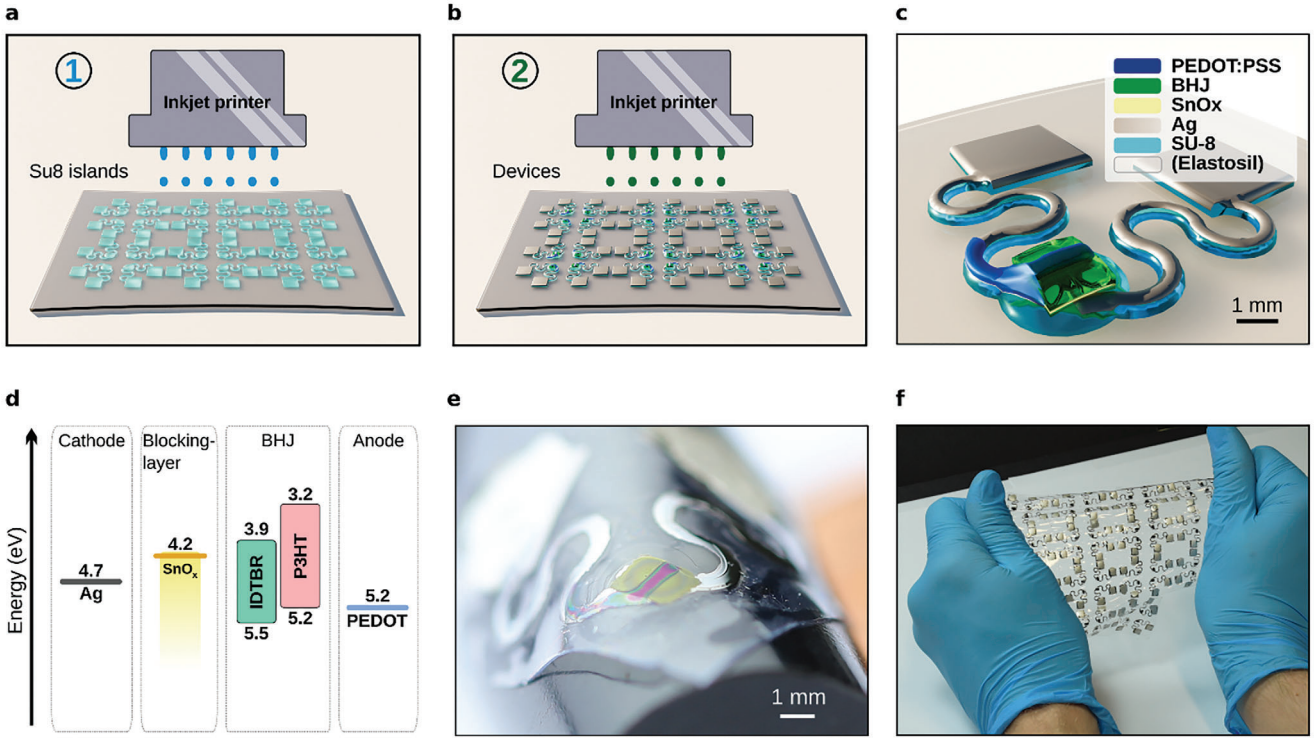

Figure 1. Inkjet-printed stretchable OPDs. a) Inkjet-printing of rigid islands with stretchable interconnects. b) Inkjet-printing of the fully printed OPDs on top of the islands. c) 3D-render of the stretchable light-sensor architecture (film thicknesses are scaled for better visualization). An OPD is printed on top of a rigid island, connected via serpentine structures to contact pads. d) Overview of the energy alignment of the used materials (adapted from the supplementary information of Ruiz-Preciado et al. CC BY[10]). e) Fully printed device placed on a curved surface with radius r = 5 mm. f) Demonstration of the bendability and stretchability of the sensor array.

we printed immediately after performing the O_2 plasma treatment to achieve precise dimensional accuracy and also used UV pinning during printing. A representative SU-8 island and serpentine interconnects are depicted in Figure 2c. The dashed line indicates the section that was used for the profilometric measurements shown in Figure 2d. By printing two layers of SU-8, a layer thickness in the range of 40–70 µm (FWHM = 3.5 mm) was achieved favoring the homogeneity and mechanical stability of the islands. Figure 2e shows an AFM measurement of the surface of the island structure. The measured rms-roughness is <2 nm despite the higher value of the stretchable substrate below. This demonstrates the successful decoupling of the surface properties through the deployment of printed islands.

2.2. OPD Printing and Characterization

Based on these results, the printing of Ag electrodes on the island structures was investigated. Figure 2f shows a printed silver electrode with line defects. Despite the favorable surface properties of the island, such issues could not be avoided by changing the print resolution (DPI) only. If the resolution was too low, line defects remained. If the resolution was too high, the intended electrode pattern was smeared out due to the excess ink. The authors attribute these printing difficulties to the surface curvature of the island structures. This was overcome by printing the electrodes in a two-step process. For each printed Ag layer an intermediate tempering process at 55° C for 2 min was carried out prior to the final annealing at 110° C for 3 min. The first step dries the contour of the layout and prevents the ink from overwetting. In the second printing step, the silver ink preferentially wets the existing shape, resulting in a closed layer. In addition, we utilized a higher printing resolution for the second step. Figure 2f,g exemplifies this process for an Ag electrode printed at 600 DPI and 800 DPI for the first and second steps, respectively.

After treating the Ag electrodes with argon plasma for 2 s, we inkjet printed the SnO_2 hole-blocking layers and annealed them at 110 °C for 15 min. The 300 nm thick P3HT:IDTBR active layers were then inkjet printed, vacuum dried, and annealed at 110 °C for 10 min in an N_2-atmosphere. The transparent PEDOT:PSS top electrodes were inkjet-printed, allowed to dry at room temperature, and then transferred to an N_2-atmosphere for annealing 10 min at 110 °C. **Figure 3** shows the fully printed stretchable OPDs and their Figures of Merit (FOM). A close-up microscope picture of a typical device is shown in Figure 3a. Figure 3b shows an image of a substrate with multiple devices, where the devices can be cut out for characterization. The serpentine structure with Ag printed on top connects the device to the contact pads. Alignment was archived using markers (fiducials) printed with the first SU-8 layer to ensure a precise overlap of all layers. It can be seen that the overlap of the Ag bottom and transparent PEDOT:PSS top electrode defines the active area of the pixel (500 × 500 µm^2).

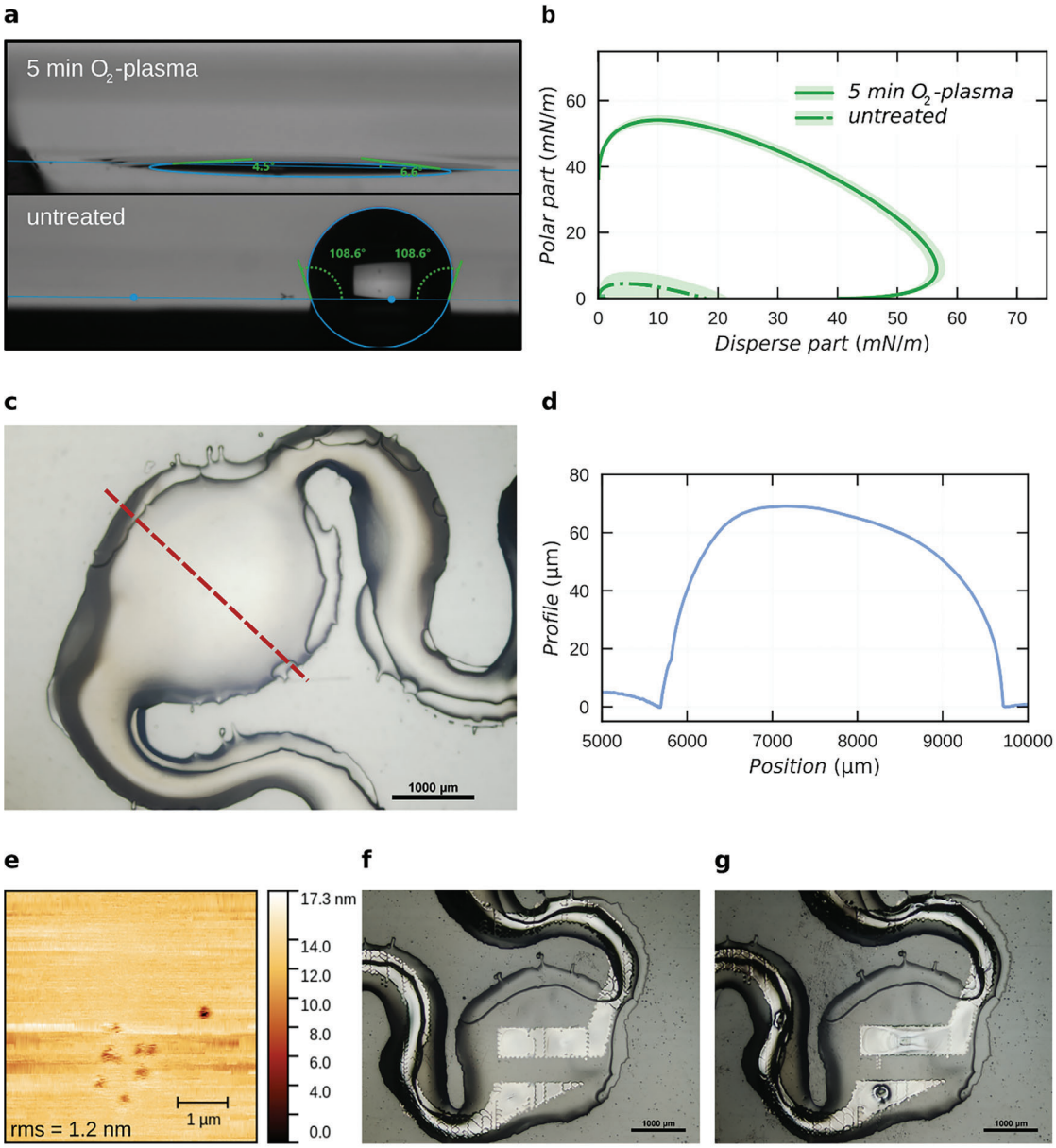

Figure 2. Surface characterization. a) Contact angle of H_2O on ELASTOSIL without (bottom) and with O_2-plasma treatment. b) Wetting envelopes (0°) of ELASTOSIL without (small envelope) and with O_2-plasma treatment. The shaded area is the standard deviation. c Microscope image of a representative SU-8 island with serpentine interconnects (printed in two passes, scale bar = 1000 µm). d) Profilometry measurement following the dashed line in the previous panel. e) AFM measurement depicting the low roughness of the SU-8 surface (scale bar = 1 µm). f) Inkjet-printed silver electrodes with line defects due to the curved surface of the structures (scale bar = 1000 µm). g) Optimized electrode—the defects were closed by printing a second Ag layer and using a two-step curing approach (scale bar = 1000 µm).

Details of the complete printing process can be found in the experimental section. As reference devices, we fabricated OPDs inkjet-printed on SU-8-coated glass using spin-coating (see Figure S3, Supporting Information). Compared to these OPDs, the stretchable devices show a higher degree of inhomogeneity in their layers. Therefore, to avoid short circuits, the active layer material was printed with a thickness of ≈300 nm and an area of 1.6 × 1.6 mm^2 (See Figure S4, Supporting Information). Figure 3c shows IV-characteristics of the fully-printed devices measured in a N_2-filled glovebox. 50% (n = 16) of the devices on the island structures showed typical photodiode behavior. Non-functional devices either had no conductive path through the serpentines or were shorted. Dark current measurements are shown with a solid line, and illuminated device measurements with a dotted line. Reference devices achieved a yield of 81% (n = 16). The average dark current of the stretchable devices, (90 ± 140) µA cm^{-2}, is significantly higher than the dark current of the reference at (0.07 ± 0.04) µA cm^{-2}. In addition, the stretchable devices have a wider dark current distribution. This indicates that the printing homogeneity on the curved surfaces needs to be further

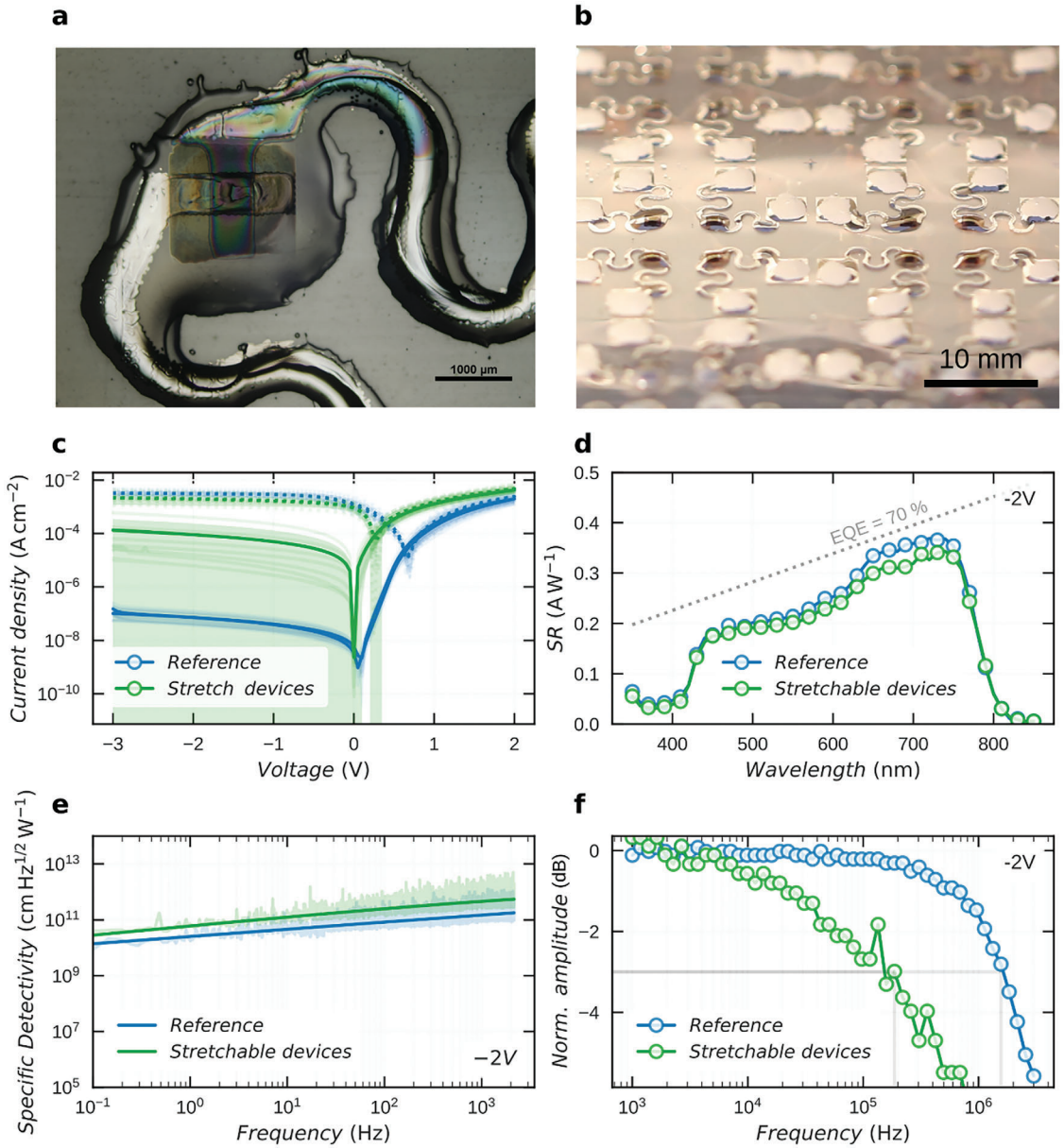

Figure 3. FOM of fully printed stretchable OPDs. a) Inkjet-printed OPD on top of an inkjet-printed island (scale bar = 1000 µm). b) Fully printed stretchable light-sensor array. The darker spots are the individual OPDs. The bright material on the contact pads is Ag-paste to improve the electrical contact to the readout (scale bar = 10 mm). c) IV-characteristics in dark (line) and illuminated (dotted line) under nitrogen atmosphere (n = 16, blue shaded area is the standard deviation). d–f) Spectral response SR, specific detectivity D* and electrical bandwidth f_{3dB} of the reference device and a representative stretchable device.

optimized as the SnO_x layer may not be completely blocking the injection current even with a nominal thickness of 30 nm.[58] In contrast to the dark current, the exhibited photocurrent for the stretchable devices of (1.9 ± 0.9) mA cm^{-2} under illumination (LED at 520 nm) is comparable to that of the reference, which gives (3.1 ± 0.9) mA cm^{-2}, demonstrating successful photoconversion.

Further FOMs were measured in ambient conditions. As the elasticity of the devices had to be maintained, epoxy and glass encapsulations were not used. Figure 3c shows the spectral responsivity of the reference sample and that of an exemplary device measured at a reverse bias of −2 V. The stretchable devices exhibited peak responsivity values (λ = 730 nm) of 340 mA W^{-1} which was slightly lower than that of the reference device, which showed 370 mA W^{-1}. The spectral fingerprint of both samples corresponds to that of typical P3HT:IDTBR devices.[63,64] Figure 3e shows the specific detectivity D* calculated from the responsivity measurements and the frequency-dependent noise density at −2 V. The D* of both samples is in the range of 10^{11} Jones, highlighting the quality of the developed process. At a frequency of 100 Hz, the reference has a higher noise (see Figure S5, Supporting Information), resulting

in a D* of 8.9 10^{10} Jones, while the stretchable sample reaches 2.8 10^{11} Jones. Finally, Figure 3f shows the dynamic response of the OPDs. Due to the inhomogeneity of the printed layers resulting from printing on the curved structures, the stretchable devices achieved a −3 dB cut-off frequency of 187 kHz, while the reference devices achieved state-of-the-art speeds of 1.56 MHz.

2.3. Mechanical Characterization

We conducted tensile tests to investigate the mechanical properties of the substrates after printing of the island and serpentines structures. **Figure** 4a shows, from left to right, tensile tests of the pristine ELASTOSIL substrate, a substrate with rigid islands but no serpentines, and a substrate with linear aligned island structures and serpentines. The pristine substrates achieved an average strain at break of (690 ± 210) %, while the substrates with islands but without serpentines achieved (175 ± 13) % and the substrates with islands and serpentines (60 ± 6) %. Figure 4b shows a representative tensile test of the two printed substrates (see also Figure S6, Supporting Information). The lower extensibility of the printed substrates can be explained by locally increased stresses at the interface of the comparatively stiffer SU-8 structures with the elastomer substrate.[30,46,65,66] To make these local stresses visible, we also performed photoelasticity imaging using cross-polarized illumination and detection (see Figure S7, Supporting Information). The results confirm that the local stresses are highest between the rigid islands and especially at the serpentine structures. However, no delamination of the island structures was observed in any of the experiments. This indicates a strong bond between the printed SU-8 and the plasma treated ELASTOSIL substrate. To verify that the rigid island structures have sufficient mechanical stability to shield the printed device from mechanical stress, microscopic images were taken at various strains (Figure 4c). The micrographs show an inkjet-printed island structure subjected to strains up to 25% where the diameter of the island structure was measured in the direction of strain. Figure 4d shows this measurement normalized by the diameter at 0% strain. For substrate strains up to 25%, the islands show elongation of only 0.62% compared to the initial state. Nevertheless, the serpentine structures showed cracks at an average strain of (14 ± 5) % at the points of higher stress (see Figure S8, Supporting Information, and the yellow arrow in Figure 4c).

These results demonstrate the success of the concept of rigid island structures and their production by inkjet-printing. However, with the objective to reach higher strains, more optimization of the geometry of the joints (e.g., triangular transitions from the islands) and the serpentine structures need to be investigated in the future. As our elasticity measurements (Figure S7, Supporting Information) and simulations from the literature[66,67] suggest, our future work will in particularly focus on reducing the local strain between the islands. This could be achieved by introducing a buffer layer between the soft and rigid materials,[15,68,69] or by using intrinsically stretchable conductors for the interconnects.[70–72] To investigate the suitability of the supporting structures for long-term performance stability, we performed cyclic conductivity measurements of printed Ag layers on top of them. This was done using the layout shown in the inset of Figure 4e, which was later used for stretchable OPDs. The symmetry axis of the layout was chosen as the strain axis. Figure 4e,f shows cyclic measurements of the resistance of printed Ag for various maximum strains. The initial resistance of the structures (150 ± 3 Ω) is shown in green. For strains of 5% there is a change in resistance corresponding to each strain cycle. However, after 500 cycles, the absolute change in resistance is reversible and is within two standard deviations of the initial value. At 10% substrate strain, a reversible cycle can be seen up to ≈150 cycles. With further cycles, the resistance begins to change permanently, and the electrical connection is lost after 450 cycles. The mechanical failure of the SU-8 serpentines is shown in Figure S8 (Supporting Information), where the formation of cracks and delamination of the structure can be observed. Such failure points are expected to disrupt the continuity of the printed Ag paths, resulting in the irreversible loss of conductivity. Thus, our systems show that a stable interconnect can be expected within the fatigue limit of serpentine (≈10% strain). To extend this limit, we plan to investigate compatible inkjet-printable materials like Ag-nanoparticles functionalized with eutectic gallium-indium[73,74] in future work. This could provide a higher degree of intrinsic stretchability to the interconnects.

2.4. Devices Under Strain

Finally, cyclic measurements of the fully-printed OPD under optical excitation were performed to test their functionality. **Figure** 5a,b shows images of OPD devices in the relaxed (0%) and strained (20%) states. A video of the experiment can also be found in Video S1 (Supporting Information). Due to thin-film interference, the devices on the island structures are clearly visible as colored areas. For these tests, the OPDs were excited with a red LED (640 nm, 45 μW cm^{-2}), whereas illumination and darkness were alternated every 20 stretching cycles. The strain applied on the sample was sequentially increased from 3% to 9% during the measurement. The axis of elongation being deliberately chosen as the axis of symmetry means that a portion of the strain is also applied to the substrate between the island structures. Thus, the strain given below represents the strain applied to the entire device. A customized open-source set-up (see Figure S9, Supporting Information) was designed and used for the tests.[75]

Figure 5c shows the measured current of the OPD as a function of mechanical cycling and optical excitation. The square-wave light signal can be easily identified for cyclic loads exceeding 600 cycles and strains up to 7%. However, after 60 strain cycles at 9%, the measurement noise increases abruptly due to the failure of the serpentine interconnects (See Figure 4c). This suggests that the OPD is still functioning, but a signal is only detected when the serpentine's contact point is established at 0%. The current response, however, displays a drift to higher values throughout the measurement. This suggests that, while not being encapsulated, the devices undergo degradation due to oxygen exposure.[76,77] This is visible in the reference measurement presented in Figure S11 (Supporting Information). In this experiment, we observe that the dark current of the OPD increases in the same time span as our cyclic measurements. This highlights the need to develop encapsulation methods for organic

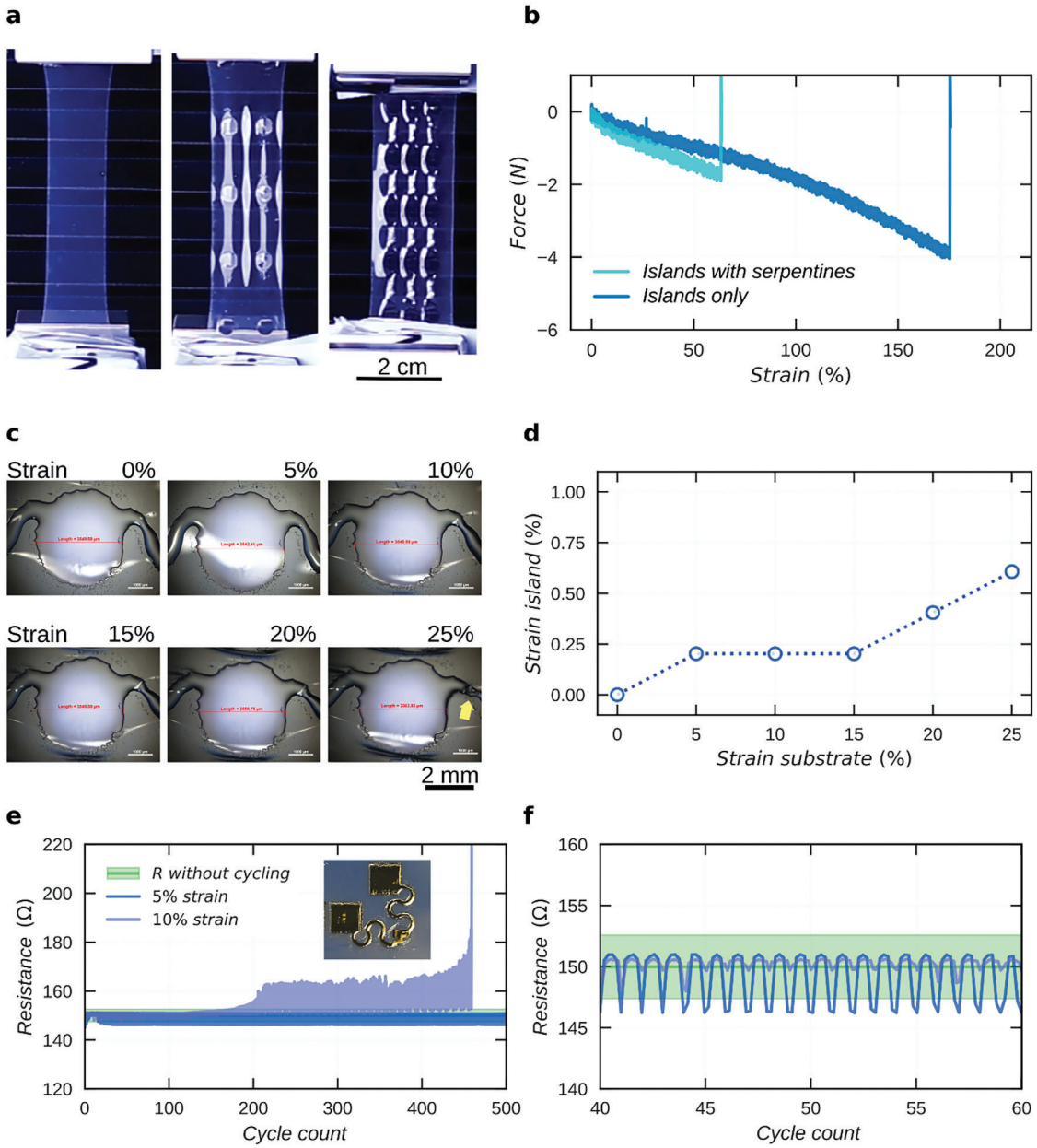

Figure 4. Mechanical properties of the islands. a) Strain test of the bare substrate (left), rigid islands without interconnects (center) and islands with serpentines (right) in a linear chain orientation (scale bar = 2 cm) b) Representative force measured during the stretching tests for the printed islands with and without serpentines (for layout and measurement of the bare substrate see Figure S6, Supporting Information) c) Stretching tests of an inkjet-printed linear chain of islands and serpentines under the microscope. The point of failure is reached when the interconnecting serpentine breaks (yellow arrow, scale bar = 2 mm). d) Relative change of the width of the island in relation to the strain of the ELASTOSIL substrate. e) Change in resistivity during cycling: Silver-ink was printed from one contact pad of the sensor layout (see inset), over the serpentines and islands, and back to the other contact pad. f) Zoom-in into the first cycles to show the reversible change in resistance. The green shaded area reflects the standard deviation of the initial resistance.

electronic materials that are compatible with our full inkjet printing process. To better analyze the performance of the OPDs under applied mechanical stress, we calculated the spectral responsivity, dividing the generated photocurrent by the incident optical power. The photocurrent was calculated by subtracting the average dark and light current measurements in subsequent cycles of the 20 measurements (see Figure S10, Supporting Information). This can also serve to decouple the oxygen degradation drift from the OPD performance. The resulting responsivity values as well as their corresponding standard deviation are shown in Figure 5d. The measured OPD exhibited an initial responsivity of (0.16 ± 0.4) AW^{-1}. In the plot it can be seen that the average responsivity value remains within the standard deviation of the previous measurement until the failure point of the serpentines

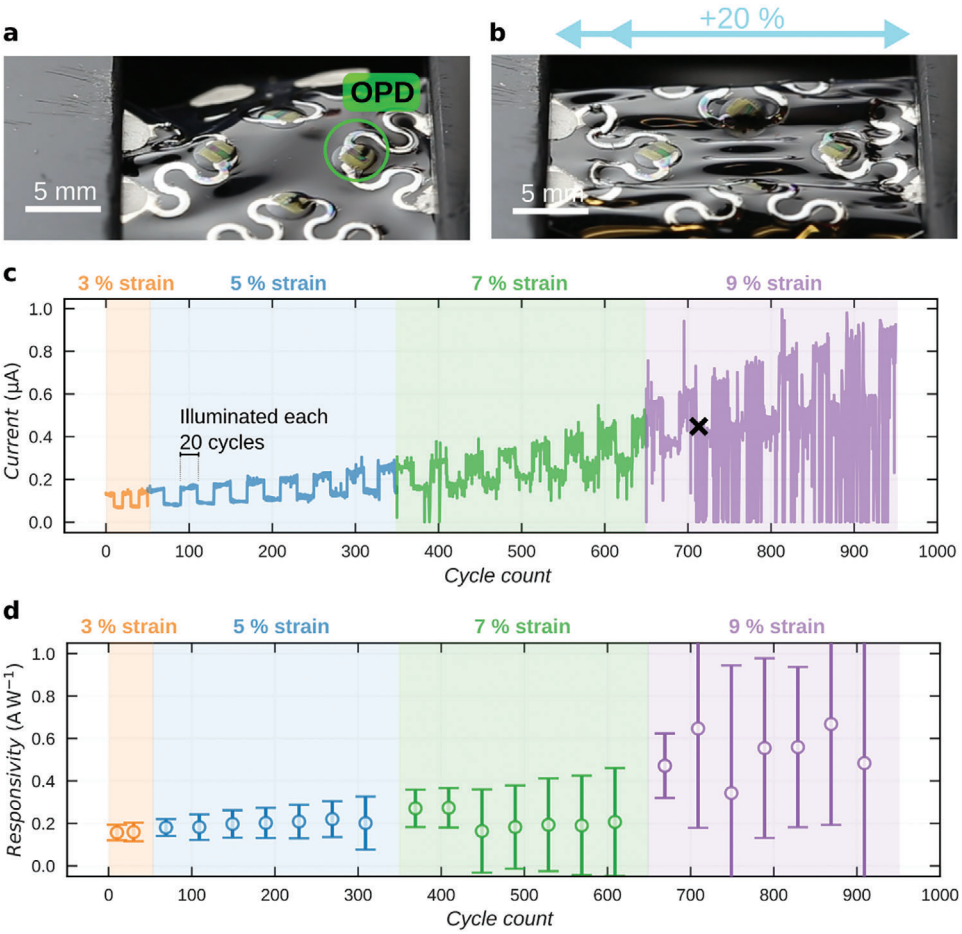

Figure 5. Devices under strain. a,b) Fully-printed stretchable light sensors relaxed and under strain. The device on the right (green circle) is connected via copper tape under the clamping mechanism of the substrate holder. c) Measured current of a square light signal measured under mechanical stretching for different strains: The stretchable device is cycled mechanically while illuminated repeatably for 20 cycles with a constant irradiance (20 cycles illuminated and 20 cycles dark). The maximum strain is increased stepwise after a fixed amount of mechanical cycles from 3% up to 9% strain. d) Calculated Responsivities for successive 20 cycles under illumination and 20 cycles in the dark. The corresponding standard deviations were summed to give the total standard deviation for each point (propagation of uncertainty).

at 9% strain. This shows that the performance of the OPD remains constant during applied mechanical stress. It confirms the efficient decoupling from the deformation of the stretchable substrate by the underlying rigid island structure.

3. Conclusion

The presented work introduces a streamlined and simplified method for fabricating stretchable light sensors relying solely on inkjet-printing. We demonstrate that printed SU-8 islands effectively decouple strain from the stretching of a flexible substrate and serve as a chemically resistant and mechanical rigid foundation for printed OPDs. Printing difficulties that arose while processing the Ag electrodes on the curved island surfaces were overcome by a two-step printing process. Following this, we demonstrated fully printed devices exhibiting peak responsivities ($\lambda = 730$ nm) of 340 mA W^{-1} and D* of 2.8 10^{11} Jones at 100 Hz, both measured at −2 V. Furthermore, the light sensors remained functional for over 600 mechanical stretching cycles at strains up to 7%. Based on our results, the following design guidelines can be derived for the fabrication of stretchable OPDs using our approach: Inkjet-printing of rigid islands with optimized flat surface on commercial elastomeric substrates. Inkjet printing of interconnects with optimized geometry to ensure extended stretchability. High-performance fully printed OPD architecture from inks compatible with the substrate properties. A printable and mechanically compatible encapsulation against ambient conditions is yet to be investigated. Overall, the presented work paves the way for novel optoelectronic applications where digital fabrication, device integration, and stretchability are key.

4. Experimental Section

Materials: Wacker's commercially available elastomer ELASTOSIL Film 2030 with a thickness of (100 ± 5%) µm was used as the stretchable substrate. For comparison, PDMS films (Sylgard 184 from *Dow*) were produced in-house by blade coating and the commercially available TPU-based substrate Elastollan 1185A10 was used. SU-8 2150 (Kayaku Advanced Materials) was diluted with Cyclopentanone (filtered with a 0.2 µm PTFE-filter) in a ratio of 1:4 (viscosity of 3 mPas (calculated from datasheet) and a total SFE of 34 mN m^{-1}[78]). To avoid crosslinking of

SU-8, processes were performed in a yellow-room. The electrodes were printed with a commercially available 30–35 wt% Ag nanoparticle ink (Sigma–Aldrich TGME Silver Dispersion). SnO_2 nanoparticle ink (Avantama N-31) was mixed with diethylene glycol (DEG, CAS 111-46-6) in a 2:1 ratio. The BHJ consists of regioregular poly(3-hexylthiophene) (P3HT, from RIEKE Metals), dissolved in o-dichlorobenzene (at 20 g/L) and mixed 1:1 with the non-fullerene acceptor 5,5′-[[4,4,9,9-Tetraoctyl-4,9-dihydro-s-indaceno[1,2-b:5,6-b']] dithiophene-2,7-diyl]bis(2,1,3-benzothiadiazole-7,4-diylmethylidyne)]bis[3-ethyl-2-thioxo-4-thiazolidinone] (IDTBR, from 1-MATERIALS) dissolved at in o-dichlorobenzene (20 g/L). The ink was mixed in a Glovebox under N_2 atmosphere, filtered at 90 °C (lower viscosity) with a 0.45 µm polyvinylidene fluoride (PVDF) filter and degassed in an ultrasonic bath. Poly(3,4-ethylenedioxythiophene) polystyrene sulfonate (PEDOT:PSS, Clevios F HC-Solar Heraeus) was prepared with 0.3 vol% of Zonyl FS-300 (CAS 197664-69-0, Fluka analytical), filtered with a 0.45 µm PVDF filter and degassed for >15 min.

Printing of the Islands: To prepare the ELASTOSIL substrates for printing, they were cleaned by blow-drying with compressed N_2 and treated with O_2 plasma for 5 min using a DIENER plasma oven (version C). It was crucial to print on freshly treated substrates. Substrates were placed on the printing table and secured using blue adhesion tape around the edges. To eliminate surface charges, a MILTY ZEROSTAT III antistatic pistol was used. All parts of the islands and OPDs were printed on a Pixdro LP50 (SUSS MicroTec). The rigid island and serpentine structures were printed using the industrial Fujifilm Spectra printhead (SM-128-AA, 128 50 pL nozzles). In a first printing step, the SU-8 ink was printed at 1500 DPI print resolution and a frequency of 3 kHz. During the printing process, a UV lamp was used (UV-pinning). The sample was then placed on a hotplate at 95 °C for 120 s (soft bake). Next, the sample was cured using a 365 nm UV LED for 300 s. Another baking step was done at 95 °C for 300 s, followed by a final hard bake at 110 °C for 15 min. A second SU-8 layer was printed on top to reach higher thicknesses. The second printing was identical to the first step, with the exception that no UV pinning was used during the printing process. During curing and baking, metal weights were laid on the edges of the substrates to avoid bending.

Printing Ag Electrodes on Curved Surface: The Ag electrodes were fabricated using a Spectra QS-256/10 (10 PL with 256 nozzels, Fujifilm) in two printing steps resulting in a total thickness of ≈300 nm. Each step was preceded by treatment with an antistatic gun (MILTY ZEROSTAT III). In the first printing step, 2 s O_2 plasma was used to prepare the SU-8 surface and printed at room temperature with 600–650 DPI at 2 kHz. To anneal the Ag, the samples were placed on a hotplate at 55° C for 2 min (partial drying and pinning of the outer shape) and another hotplate at 110° C for 3 min (sintering). The second printing step was also conducted at room temperature but without prior O_2 plasma and with 800 DPI at 2 kHz, followed by the same annealing step at 55° C and 110° C. To increase the connectivity even further, the Ag could be printed on the serpentines in a third, separate step (e.g., 1400 DPI at 2 kHz and annealing for 5 min at 110° C only) in the future.

Printing of the OPD Layers: The subsequent OPD layers were all printed with Fujifilm Dimatix cartridges (DMC 10 pL, 16 nozzles). SnO_2 hole-blocking layers were inkjet-printed with 750 DPI and 1 kHz (≈30 nm thickness) on top of the Ag, after the electrodes were treated with 2 s Argon plasma. The samples were then annealed at 110 °C for 15 min. P3HT:IDTBR active layers were printed with 1500 DPI at 1000 Hz (≈300 nm thickness) and dried using vacuum drying. To avoid degradation, a maximum of 16 devices was printed in one run before transferring the samples into N_2-atmosphere for annealing (10 min at 110 °C). The transparent PEDOT:PSS top electrodes were inkjet-printed with 1500 DPI at 1 kHz (≈700 nm thickness). To avoid clogging of the printhead, it was continuously operating at 5 Hz while idle. The devices were first left to dry at room temperature before transferred into N_2 atmosphere for annealing (110 °C for 10 min).

Surface Measurements and Mechanical Characterization Islands: Roughness (rms) measurements and layer thicknesses were determined by profilometry (Bruker, Dektak 150). Contact angles of H_2O, diiodomethane and ethylene glycol were measured with a Krüss DSA 100 to estimate the surface energies of the substrates and to calculate the wetting envelopes. To mechanically characterize the substrates and island structures, tensile tests were carried out using the Alluris FMT-310BU universal testing machine. Microscope pictures under strain were recorded by clamping the flexible substrates in a holder accessory of Krüss DSA 100 that features a screw for linear stretching. The substrate strain was manually measured, and the elongation of the SU-8 island was detected by the software of the microscope.

Optoelectronic Characterization Stretchable OPDs: IV-characterization was performed with an Agilent 4155 C semiconductor parameter analyzer under nitrogen atmosphere (glovebox). For IV-measurements under illumination, a green LED (λ = 520 nm) was used as a light source. An in-detail description of the setup used for responsivity measurements (450 W OSRAM XBO Xenon discharge lamp, monochromator (Acton SP-2150i), chopper wheel (173 Hz), amplifier (Femto DHPCA-100) and SR830 lock-in amplifier) as well as bandwidth measurements (Oxxius LBX520 LASER with square-light signal of varying frequency (function generator Agilent 33 522 A) and oscilloscope (Agilent DSO 6102 A) can be found in the PhD thesis of N. Strobel.[79] The noise spectral density (Sn(f)) was measured by recording a time dependent dark current in a custom-built shielded box to avoid pickup noise and calculating the frequency dependent Sn(f) via Fourier-transformation. Details of the setup and calculations (transimpedance amplifier (TIA, FEMTO DLPCA-200), the isolated voltage source (SIM928, SRS), the SMU (Keithley 2636 A), a Hann window function and NUFFT) can be found in the first author's PhD thesis.[53] To calculate D*, a custom python module[80] was used that combines corresponding SR measurements (at 780 nm), Sn(f), as well as the area of the OPDs.

Mechanical cycling and optical excitation of the stretchable OPDs were performed with a customized open-source set-up (see Figure S9, Supporting Information[75]) and a red high-power LED (640 nm) at 40 mm distance (145 µW/cm^{-1}). The optical signal was matched with the mechanical cycles (20 cycles in dark followed by 20 cycles under illumination) and the samples were periodically stretched with a velocity of 3 mm s^{-1}. The readout of the OPD signal was conducted with a Keithley 2636A SMU (for the script see[75]).

Statistical analysis: Data was used as measured by the instruments. Only in the case of noise measurements a window function was applied to account for errors of the DFT calculation. Where applicable data is presented as lines with a shaded area or error-bar to represent the mean ± 1σ standard deviation. Statistics on stretchable and reference devices were conducted with an sample size of n = 16 each. A custom python module for the experimental evaluation was programmed utilizing standard python libraries of the field like numpy, pandas, mathplotlib and astropy. It has been released under a creative commons license (see code availability).

Supporting Information

Supporting Information is available from the Wiley Online Library or from the author.

Acknowledgements

This work was supported by the Deutsche Forschungsgemeinschaft (DFG, German Research Foundation) project HE 7056/6-1 and under Germany's Strategy via the Excellence Cluster 3D Matter Made to Order (3DMM2O, EXC-2082/1-390761711). G.H.S. thanks the DFG (Heisenbergprofessur, HE 7056/7-1) for the financial support. K.X. thanks the Carl Zeiss Foundation for the financial support. M. S. is grateful for the financial support and mentoring from the German Academic Scholarship Foundation. Parts of this work and preliminary experiments can also be found in M. S. dissertation.[53] The authors thank T. Scott for proofreading. The authors utilized language software to improve the readability of the manuscript.[81] The authors acknowledge support by the KIT-Publication Fund of the Karlsruhe Institute of Technology.

Open access funding enabled and organized by Projekt DEAL.

Conflict of Interest

The authors declare no conflict of interest.

Author Contributions

M.S. and G.H.-S. conceived and coordinated the research. G.H.-S. and U.L. provided funding and supervised the research. M.S. conducted or contributed to all experiments and build/programmed research software and hardware. C.R., L.A.R.-P., P.K., and S.S. conducted or contributed to inkjet-printing of the different layers. C.R. conducted mechanical testing. L.S. contributed to material evaluation and selection as well as to preliminary experiments. A.P. conducted photoelasticity measurements. K.X. took photographs and contributed to material processing. M.S. and G.H.-S. analyzed the data and discussed the results. M.S. and G.H.-S. wrote the manuscript. All authors discussed ideas and reviewed and approved the manuscript.

Data Availability Statement

The data supporting the findings of this study are available from the corresponding authors upon reasonable request. The underlying code for this study is available in KITopen and RADAR4KIT and can be accessed via https://doi.org/10.5445/IR/1000156174 and https://dx.doi.org/10.35097/1839.

Keywords

elastomeric substrates, inkjet-printing, organic photodiodes, rigid platforms, stretchable electronics

Received: August 27, 2024
Revised: December 12, 2024
Published online:

[1] I. Yun, *Photodiodes – From Fundamentals to Applications*, InTech, UK **2012**.
[2] B. Nabet, *Photodetectors: Materials, Devices and Applications*, Elsevier, Amsterdam, **2016**.
[3] S. Donati, *Meas. Sci. Technol.* **2001**, *12*, 653.
[4] N. Strobel, M. Seiberlich, R. Eckstein, U. Lemmer, G. H. Sosa, *Flex. Print. Electron.* **2019**, *4*, 043001.
[5] J. Kim, C. Son, S. Lee, S. Kim, *Adv. Mater. Technol.* **2024**, *9*, 2301468.
[6] C. Li, H. Luo, X. Lin, S. Zhang, J. Song, *Proc. Natl. Acad. Sci. USA* **2024**, *121*, 2318739121.
[7] Y. Khan, D. Han, A. Pierre, J. Ting, X. Wang, C. M. Lochner, G. Bovo, N. Yaacobi-Gross, C. Newsome, R. Wilson, A. C. Arias, *Proc. Natl. Acad. Sci. USA* **2018**, *115*, E11015.
[8] T. Yokota, P. Zalar, M. Kaltenbrunner, H. Jinno, N. Matsuhisa, H. Kitanosako, Y. Tachibana, W. Yukita, M. Koizumi, T. Someya, *Sci. Adv.* **2016**, *2*, 1501856.
[9] N. Strobel, N. Droseros, W. Köntges, M. Seiberlich, M. Pietsch, S. Schlisske, F. Lindheimer, R. R. Schröder, U. Lemmer, M. Pfannmöller, N. Banerji, G. Hernandez-Sosa, *Adv. Mater.* **2020**, *32*, 1908258.
[10] L. A. Ruiz-Preciado, S. Baek, N. Strobel, K. Xia, M. Seiberlich, S. Park, U. Lemmer, S. Jung, G. Hernandez-Sosa, *npj Flex. Electron* **2023**, *7*, 6.
[11] B. Bao, D. D. Karnaushenko, O. G. Schmidt, Y. Song, D. Karnaushenko, *Adv. Intell. Sys.* **2022**, *4*, 2100253.
[12] D. Cherian, K. Y. Mitra, M. Hartwig, P. E. Malinowski, R. R. Baumann, *IEEE Sens. J.* **2018**, *18*, 94.
[13] V. Vallem, Y. Sargolzaeiaval, M. Ozturk, Y.-C. Lai, M. D. Dickey, *Adv. Mater.* **2021**, *33*, 2004832.
[14] H. Xu, L. Yin, C. Liu, X. Sheng, N. Zhao, *Adv. Mater.* **2018**, *30*, 1800156.
[15] J. Kang, J. Mun, Y. Zheng, M. Koizumi, N. Matsuhisa, H.-C. Wu, S. Chen, J. B.-H. Tok, G. H. Lee, L. Jin, Z. Bao, *Nat. Nanotechnol.* **2022**, *17*, 1265.
[16] H. Cho, B. Lee, D. Jang, J. Yoon, S. Chung, Y. Hong, *Mater. Horiz.* **2022**, *9*, 2053.
[17] S. Wang, J. Xu, W. Wang, G.-J. N. Wang, R. Rastak, F. Molina-Lopez, J. W. Chung, S. Niu, V. R. Feig, J. Lopez, T. Lei, S.-K. Kwon, Y. Kim, A. M. Foudeh, A. Ehrlich, A. Gasperini, Y. Yun, B. Murmann, J. B.-H. Tok, Z. Bao, *Nature* **2018**, *555*, 83.
[18] M. Kaltenbrunner, M. S. White, E. D. Głowacki, T. Sekitani, T. Someya, N. S. Sariciftci, S. Bauer, *Nat. Commun.* **2012**, *3*, 770.
[19] S. Park, K. Fukuda, M. Wang, C. Lee, T. Yokota, H. Jin, H. Jinno, H. Kimura, P. Zalar, N. Matsuhisa, S. Umezu, G. C. Bazan, T. Someya, *Adv. Mater.* **2018**, *30*, 1802359.
[20] Z. Jiang, K. Yu, H. Wang, S. Rich, T. Yokota, K. Fukuda, T. Someya, *Adv. Mater. Technol.* **2021**, *6*, 2000956.
[21] N. Matsuhisa, S. Niu, S. J. K. O'Neill, J. Kang, Y. Ochiai, T. Katsumata, H.-C. Wu, M. Ashizawa, G.-J. N. Wang, D. Zhong, X. Wang, X. Gong, R. Ning, H. Gong, I. You, Y. Zheng, Z. Zhang, J. B.-H. Tok, X. Chen, Z. Bao, *Nature* **2021**, *600*, 246.
[22] J. Liu, J. Wang, Z. Zhang, F. Molina-Lopez, G.-J. N. Wang, B. C. Schroeder, X. Yan, Y. Zeng, O. Zhao, H. Tran, T. Lei, Y. Lu, Y.-X. Wang, J. B.-H. Tok, R. Dauskardt, J. W. Chung, Y. Yun, Z. Bao, *Nat. Commun.* **2020**, *11*, 3362.
[23] Z. Zhang, W. Wang, Y. Jiang, Y.-X. Wang, Y. Wu, J.-C. Lai, S. Niu, C. Xu, C.-C. Shih, C. Wang, H. Yan, L. Galuska, N. Prine, H.-C. Wu, D. Zhong, G. Chen, N. Matsuhisa, Y. Zheng, Z. Yu, Y. Wang, R. Dauskardt, X. Gu, J. B.-H. Tok, Z. Bao, *Nature* **2022**, *603*, 624.
[24] J.-K. Song, J. Kim, J. Yoon, J. H. Koo, H. Jung, K. Kang, S.-H. Sunwoo, S. Yoo, H. Chang, J. Jo, W. Baek, S. Lee, M. Lee, H. J. Kim, M. Shin, Y. J. Yoo, Y. M. Song, T. Hyeon, D.-H. Kim, D. Son, *Nat. Nanotechnol.* **2022**, *17*, 849.
[25] D.-H. Lien, H.-P. Wang, S.-B. Chen, Y.-C. Chi, C.-L. Wu, G.-R. Lin, Y.-C. Liao, J.-H. He, *npj Flex. Electron* **2018**, *2*, 19.
[26] H. Kang, Y. Lee, G. H. Lee, J. W. Chung, Y.-N. Kwon, J.-Y. Kim, Y. Kuzumoto, S. Gam, S.-G. Kang, J. Y. Jung, A. Choi, Y. Yun, *Adv. Funct. Mater.* **2023**, *33*, 2212219.
[27] Y. Gao, J. Liao, H. Chen, H. Ning, Q. Wu, Z. Li, Z. Wang, X. Zhang, M. Shao, Y. Yu, *Adv. Sci.* **2023**, *10*, 2204727.
[28] N. Cui, Y. Song, C.-H. Tan, K. Zhang, X. Yang, S. Dong, B. Xie, F. Huang, *npj Flex Electron* **2021**, *5*, 31.
[29] Y. Park, C. Fuentes-Hernandez, K. Kim, W.-F. Chou, F. A. Larrain, S. Graham, O. N. Pierron, B. Kippelen, *Sci. Adv.* **2021**, *7*, eabj6565.
[30] Y. Lim, J. Yoon, J. Yun, D. Kim, S. Y. Hong, S.-J. Lee, G. Zi, J. S. Ha, *ACS Nano* **2014**, *8*, 11639.
[31] T. Sekitani, Y. Noguchi, K. Hata, T. Fukushima, T. Aida, T. Someya, *Science* **2008**, *321*, 1468.
[32] Q. Hua, J. Sun, H. Liu, R. Bao, R. Yu, J. Zhai, C. Pan, Z. L. Wang, *Nat. Commun.* **2018**, *9*, 244.
[33] S.-I. Park, Y. Xiong, R.-H. Kim, P. Elvikis, M. Meitl, D.-H. Kim, J. Wu, J. Yoon, C.-J. Yu, Z. Liu, Y. Huang, K. Hwang, P. Ferreira, X. Li, K. Choquette, J. A. Rogers, *Science* **2009**, *325*, 977.
[34] H. C. Ko, G. Shin, S. Wang, M. P. Stoykovich, J. W. Lee, D.-H. Kim, J. S. Ha, Y. Huang, K.-C. Hwang, J. A. Rogers, *Small* **2009**, *5*, 2703.
[35] J. Lee, J. Wu, M. Shi, J. Yoon, S.-I. Park, M. Li, Z. Liu, Y. Huang, J. A. Rogers, *Adv. Mater.* **2011**, *23*, 986.
[36] D.-H. Kim, N. Lu, R. Ghaffari, Y.-S. Kim, S. P. Lee, L. Xu, J. Wu, R. H. Kim, J. Song, Z. Liu, J. Viventi, B. de Graff, B. Elolampi, M. Mansour, M. J. Slepian, S. Hwang, J. D. Moss, S.-M. Won, Y. Huang, B. Litt, J. A. Rogers, *Nat. Mater.* **2011**, *10*, 316.

[37] L. Xu, S. R. Gutbrod, A. P. Bonifas, Y. Su, M. S. Sulkin, N. Lu, H.-J. Chung, K.-I. Jang, Z. Liu, M. Ying, C. Lu, R. C. Webb, J.-S. Kim, J. I. Laughner, H. Cheng, Y. Liu, A. Ameen, J.-W. Jeong, G.-T. Kim, Y. Huang, I. R. Efimov, J. A. Rogers, *Nat. Commun.* **2014**, *5*, 3329.
[38] D. Ruh, P. Reith, S. Sherman, M. Theodor, J. Ruhhammer, A. Seifert, H. Zappe, *Adv. Mater.* **2014**, *26*, 1706.
[39] J. Kim, M. Lee, H. J. Shim, R. Ghaffari, H. R. Cho, D. Son, Y. H. Jung, M. Soh, C. Choi, S. Jung, K. Chu, D. Jeon, S.-T. Lee, J. H. Kim, S. H. Choi, T. Hyeon, D.-H. Kim, *Nat. Commun.* **2014**, *5*, 5747.
[40] M. Cai, S. Nie, Y. Du, C. Wang, J. Song, *ACS Appl. Mater. Interfaces* **2019**, *11*, 14340.
[41] Y. Lee, J. W. Chung, G. H. Lee, H. Kang, J.-Y. Kim, C. Bae, H. Yoo, S. Jeong, H. Cho, S.-G. Kang, J. Y. Jung, D.-W. Lee, S. Gam, S. G. Hahm, Y. Kuzumoto, S. J. Kim, Z. Bao, Y. Hong, Y. Yun, S. Kim, *Sci. Adv.* **2021**, *7*, eabg9180.
[42] M. Ku, J. Kim, J.-E. Won, W. Kang, Y.-G. Park, J. Park, J.-H. Lee, J. Cheon, H. H. Lee, J.-U. Park, *Sci. Adv.* **2020**, *6*, eabb2891.
[43] M. Held, A. Pichler, J. Chabeda, N. Lam, P. Hindenberg, C. Romero-Nieto, G. Hernandez-Sosa, *Adv. Sustainable Syst.* **2021**, *6*, 2100035.
[44] C. A. Silva, J. Lv, L. Yin, I. Jeerapan, G. Innocenzi, F. Soto, Y.-G. Ha, J. Wang, *Adv. Funct. Mater.* **2020**, *30*, 2002041.
[45] N. Matsuhisa, M. Kaltenbrunner, T. Yokota, H. Jinno, K. Kuribara, T. Sekitani, T. Someya, *Nat. Commun.* **2015**, *6*, 7461.
[46] B. Lee, J. Byun, E. Oh, H. Kim, S. Kim, Y. Hong, *SID Symp. Digest Tech. Papers* **2016**, *47*, 672.
[47] N. Matsuhisa, D. Inoue, P. Zalar, H. Jin, Y. Matsuba, A. Itoh, T. Yokota, D. Hashizume, T. Someya, *Nat. Mater.* **2017**, *16*, 834.
[48] M. Pietsch, S. Schlisske, M. Held, P. Maag, G. Hernandez-Sosa, *Flex. Print. Electron.* **2022**, *7*, 025007.
[49] E. Oh, J. Byun, B. Lee, S. Kim, D. Kim, J. Yoon, Y. Hong, *Adv. Electronic Mater.* **2017**, *3*, 1600517.
[50] J. Byun, B. Lee, E. Oh, H. Kim, S. Kim, S. Lee, Y. Hong, *Sci. Rep.* **2017**, *7*, 45328.
[51] J. Byun, E. Oh, B. Lee, S. Kim, S. Lee, Y. Hong, *Adv. Funct. Mater.* **2017**, *27*, 1701912.
[52] J. Byun, S. Chung, Y. Hong, *Adv. Mater.* **2018**, *30*, 1802190.
[53] M. Seiberlich, "Gedruckte Organische Fotodioden: Rauschreduktion, Abstandsmessungen und dehnbare Lichtsensoren," https://doi.org/10.5445/IR/1000169380 can be found under https://publikationen.bibliothek.kit.edu/1000169380, **2024**.
[54] Z. Chen, J.-B. Lee, *Micromachines* **2021**, *12*, 794.
[55] Q. Zhang, M. Schambach, S. Schlisske, Q. Jin, A. Mertens, C. Rainer, G. Hernandez-Sosa, M. Heizmann, U. Lemmer, *Adv. Opt. Mater.* **2022**, *10*, 2200677.
[56] M. Seiberlich, Q. Zhang, A. V. Tunc, K. Xia, L. A. Ruiz-Preciado, S. Schlisske, K. Falis, N. Strobel, U. Lemmer, G. Hernandez-Sosa, *Adv. Sens. Res.* **2023**, *2*, 2300004.
[57] L. A. Ruiz-Preciado, P. Pešek, C. Guerra-Yánez, Z. Ghassemlooy, S. Zvánovec, G. Hernandez-Sosa, *Sci. Rep.* **2024**, *14*, 3296.
[58] P. Krebsbach, S. Schlisske, N. Strobel, M. Seiberlich, L. A. Ruiz-Preciado, C. Rainer, X. Huang, U. Lemmer, G. Hernandez-Sosa, *ACS Appl. Electron. Mater.* **2021**, *3*, 4959.
[59] M. Seiberlich, N. Strobel, L. A. Ruiz-Preciado, M. Ruscello, U. Lemmer, G. Hernandez-Sosa, *Adv. Electron. Mater.* **2021**, *7*, 2000811.
[60] D. H. Kaelble, *J. Adhes.* **1970**, *2*, 66.
[61] D. K. Owens, R. C. Wendt, *J. Appl. Polym. Sci.* **1969**, *13*, 1741.
[62] S. Schlißke, Substratfunktionalisierungen zur Optimierung tintenstrahlgedruckter opto-elektronischer Bauteile, Karlsruher Institut für Technologie (KIT), germany, **2021**, p. 160, https://doi.org/10.5445/IR/1000130024.
[63] N. Strobel, M. Seiberlich, T. Rödlmeier, U. Lemmer, G. Hernandez-Sosa, *ACS Appl. Mater. Interfaces* **2018**, *10*, 42733,.
[64] N. Gasparini, A. Gregori, M. Salvador, M. Biele, A. Wadsworth, S. Tedde, D. Baran, I. McCulloch, C. J. Brabec, *Adv. Mater. Technol.* **2018**, *3*, 1800104.
[65] A. Romeo, Q. Liu, Z. Suo, S. P. Lacour, *Appl. Phys. Lett.* **2013**, *102*, 131904.
[66] T. Pan, M. Pharr, Y. Ma, R. Ning, Z. Yan, R. Xu, X. Feng, Y. Huang, J. A. Rogers, *Adv. Funct. Mater.* **2017**, *27*, 1702589.
[67] C. Ye, C. I. Ume, S. K. Sitaraman, *J. Electron. Packag.* **2020**, *142*, 021007.
[68] T. Kim, H. Lee, W. Jo, T. Kim, S. Yoo, *Adv. Mater. Technol.* **2020**, *5*, 2000494.
[69] Y. Wang, C. Zhu, R. Pfattner, H. Yan, L. Jin, S. Chen, F. Molina-Lopez, F. Lissel, J. Liu, N. I. Rabiah, Z. Chen, J. W. Chung, C. Linder, M. F. Toney, B. Murmann, Z. Bao, *Sci. Adv.* **2017**, *3*, 1602076.
[70] M. Amjadi, Y. J. Yoon, I. Park, *Nanotechnology* **2015**, *26*, 375501.
[71] S. Liu, D. S. Shah, R. Kramer-Bottiglio, *Nat. Mater.* **2021**, *20*, 851.
[72] Y. Jiang, S. Ji, J. Sun, J. Huang, Y. Li, G. Zou, T. Salim, C. Wang, W. Li, H. Jin, J. Xu, S. Wang, T. Lei, X. Yan, W. Y. X. Peh, S.-C. Yen, Z. Liu, M. Yu, H. Zhao, Z. Lu, G. Li, H. Gao, Z. Liu, Z. Bao, X. Chen, *Nature* **2023**, *614*, 456.
[73] M. Tavakoli, M. H. Malakooti, H. Paisana, Y. Ohm, D. Green Marques, P. Alhais Lopes, A. P. Piedade, A. T. de Almeida, C. Majidi, *Adv. Mater.* **2018**, *30*, 1801852.
[74] A. F. Silva, H. Paisana, T. Fernandes, J. Góis, A. Serra, J. F. J. Coelho, A. T. de Almeida, C. Majidi, M. Tavakoli, *Adv. Mater. Technol.* **2020**, *5*, 2000343.
[75] M. Seiberlich, K. Falis, G. H. Sosa, Modular linear experiment stage, Karlsruhe Institute of Technology, USA, **2023**.
[76] Z. Lan, M.-H. Lee, F. Zhu, *Adv. Intell. Syst.* **2022**, *4*, 2100167.
[77] A. Falco, P. Lugli, F. C. Loghin, M. Bobinger, M. Gerlt, in *2017 IEEE 17th Int. Conf. on Nanotechnology (IEEE-NANO)*, IEEE, New York **2017**, pp. 522.
[78] M. Robin, W. Kuai, M. Amela-Cortes, S. Cordier, Y. Molard, T. Mohammed-Brahim, E. Jacques, M. Harnois, *ACS Appl. Mater. Interfaces* **2015**, *7*, 21975.
[79] N. Strobel, Printed Organic Photodiodes with Enhanced Performance and Simplified Processing, Karlsruher Institut für Technologie (KIT), USA, **2020**, p. 150.
[80] M. Seiberlich, Q. Zhang, A. V. Tunc, K. Xia, L. A. Ruiz-Preciado, S. Schlisske, K. Falis, N. Strobel, U. Lemmer, G. Hernandez-Sosa, *Adv. Sensor Res.* **2023**, *2*, 2300004.
[81] "DeepL Terms and Conditions," can be found under https://www.deepl.com/pro-license.